J Mol Model (2012) 18:5035–5040
DOI 10.1007/s00894-012-1510-4

ORIGINAL PAPER

First principles study of periodic size dependent band gap variation of Cu doped ZnO single-wall nanotube

Dong Mei Song · Tong Hui Wang · Jian Chen Li

Received: 24 April 2012 / Accepted: 14 June 2012 / Published online: 3 July 2012

Abstract In this contribution, the size dependent band gap variation of $(Zn_{4/6}Cu_{2/6}O)_L/(Zn_{5/6}Cu_{1/6}O)_L$ (L is the periodic size) superlattices are investigated with the change of L. The results show that the variation tendency of band gap appears a minimum in S_4 (L=4) which is nearly a conductor. The band gap of S_3 (L=3) and S_5 (L=5) also decrease obviously compared to the other three configurations. Especially, the band gap of S_3 has decreased to 2.16 eV which is in the region of narrow bandgap semiconductor. Thus, the band gap can be modulated by alloying through constructing an appropriate variation period. Our ZnCuO superlattices can absorb light in both visible and UV region. These properties make the superlattices a potential application in photocatalysis and the visible light emitter.

Keywords Band gap · Density functional theory · Interface · SWNTs

Introduction

ZnO is a geometrically versatile II-VI semiconductor material that can form nanodots [1], nanorods [2], nanowires [3], nanobelts [4], nanotubes [5], and nanobridges [6]. ZnO is a direct band gap (E_g=3.37 eV) semiconductor with a large exciton binding energy (60 meV), exhibiting near-UV emission, transparent conductivity, and piezoelectricity. Because of its favorable characteristics, ZnO has received considerable attention over the past few years [7–11].

D. M. Song · T. H. Wang · J. C. Li (✉)
Key laboratory of Automobile Materials, Ministry of Educations, and Department of Materials Science and Engineering, Jilin University, Changchun 130022, China
e-mail: ljc@jlu.edu.cn

Micro- and nanoscale structures have attracted increasing interest because their specific structures and properties differ from their bulk counterparts, and have wide applications in chemistry, biotechnology, and materials science [12–16]. As the most typical one, single-wall nanotubes (SWNTs) have remarkable characteristics of high surface/volume ratio and low density, and hence possess potential applications in many areas, such as dye-sensitized photovoltaic cells, dimensionally stable anodes, metal-ion batteries, electrochemical supercapacitors, hydrogen storage devices, biosensors, and gas sensors [17–21].

Transition metal oxide based photo-electrochemical splitting of water has attracted wide interest since the photo-induced decomposition of water on TiO_2 electrodes was discovered. ZnO has a similar band gap width and band edge position of TiO_2. Meanwhile, the typical electron mobility of ZnO is 10-100 times lager than that of TiO_2. However, this wide band gap can collect only about 5 % incident solar spectrum energy in UV region. Recently, a novel $(Zn_{4/6}Cu_{2/6}O)_3/(Zn_{5/6}Cu_{1/6}O)_3$ superlattice has been modeled [22], whose band gap E_g is 2.16 eV and collection ability is 42 % of the incident solar spectrum energy. In addition, to satisfy the water splitting redox requirement, the oxygen and hydrogen reactions must lie between the valence band maximum (VBM) and conduction band minimum (CBM) of photocatalysis. A single-wall ZnO nanotube (SWZONT) (higher porosity, low density and larger surface-volume ratio) has been forecasted to possibly be fabricated because of its negative binding energy and a possible scheme is proposed to achieve the SWZONTs from the solid-vapor phase process with carbon nanotubes as templates [23]. While, for one-dimensional ZnO nanostructures, a tube should be more stable than a wire, which also supports the above viewpoints [24]. Recently, multi-walled ZnO nanotubes have been fabricated via different techniques, such as a thermal reduction route using ZnS power as

source material, synthesized on a Si wafer coated with a thin ZnO film, and so on [20, 25].Moreover, the Cu-ZnO nanowire and nanotube have been synthesized by electrodeposition for catalyzing higher alcohols from syngas [26]. Thus, our established superlattice nanotubes should be fabricated experimentally. Therefore, the band gap design is related to a superlattice structure wherein there exist a Cu concentration variation and a coherent interface.

The above structures are closely related to the interfacial effect [27, 28]. However, it is difficult to characterize the geometric and electronic properties of interface by experiments due to their complexity. Thus, the computational methods have become a powerful research tool to provide information at the atomic and electronic levels. In particular, density functional theory (DFT) calculations are widely utilized to realize the above purpose with enough accuracy.

To further decrease the wide band gap of ZnO SWNT for the application in photocatalysis and the visible light emitter, we do a further study about the superlattice. And in order to further consider the physical essence of the superlattice, the periodic superlattices with different size and same doping concentration gradient are discussed in this contribution. It can be concluded that with the same ratio of Zn, Cu and O, the E_g of the configurations L=3 and L=4 are different from the other configurations due to the effect of the middle layer inducing the rapid VBM increasing or CBM decreasing.

Simulation details

The calculations are based on the ultrasoft and norm-conserving pseudopotentials available in the CASTEP code to optimize the models and obtain authentic optical properties [29–31]. Integrations in the Brillouin zone are performed using k points of $1\times1\times6$ mesh parameter grid. Exchange and correlation effects are described by the Perdew-Burke-Eruzerhof (PBE) scheme in the generalized gradient approximation (GGA) [32]. Spin polarization is checked in the calculation since there is spin polarization exciting in ZnO/CuO system [33].

The structures of superlattices named S_1 to S_6 are shown in Fig. 1. Each configuration has two periodic units (U1 in left and U2 in right) with the same composition, which have a half of Zn-O layers (L) of the whole tube where L is 1 to 6 named S_1 to S_6. Each Zn-O layer has two single layers, namely, Zn/Cu and O layers. In U1, one Zn atom is substituted by a Cu atom per layer, while two Zn atoms are substituted by two Cu atoms in U2. The layer is numbered from left to right as 1st, 2nd, and so on. The superlattices are placed in unit cells along [001] direction where the intertube distance is larger than 10 Å, which prevents the interaction effect from the neighboring cells effectively. The bond lengths of 1.973 Å along [100] direction and 1.992 Å along [001] direction were set from the wurtzite ZnO [34]. The geometry and indexing scheme of ZnO SWNTs are the same as carbon nanotubes. After minimizing the total energy for each structure, the average bond length is about 1.88 Å, which contracts 4.41 % compared with that in bulk. The optimized bond angle in average is 117.69°, being similar to another simulation value of 118.28° [35].

Since doping group-IB elements on Zn sites of ZnO films is stable while energies are rather high when they are doped at the interstitial sites [36], Zn sites have been selected for doping Cu. Cu is doped as dispersive as possible to drop the total energy. To avoid the interaction between Cu atoms, there is at most one Cu atom in each Zn-O hexagon.

The band gap error from GGA is induced by shallow cation-d states in semiconductors on account of their strong, spurious self-interaction [37], which could be improved by a computational expedient post-GGA method (GGA+U) [38, 39]. GGA+U was originally developed to improve the GGA description of Mott insulators by introducing Hubbard-type interactions into GGA via an adjustable Coulomb parameter U. Different U values are added on Zn-4s, Zn-3d, and O-2p orbits in our conculation. We define $E_g(x)$ as the practical energy barrier for electron transitions. As U increases from 3 to 10 eV, E_g can be effectively widened where there is an inflection point at U=4.5 eV. The simulated value by DFT-B3LYP technique shows that E_g=4.35 eV for (6,0) SWNT, and E_g=3.29 eV for bulk ZnO while the actual E_g value is 3.34 eV [40]. U=4.5 eV approaches the above values and is thus taken here. The detailed discussion of the selection of U and this figure has been discussed in our previous work [22].

Results and discussion

The curve of E_g as a function of L is shown in Fig. 2a. When L<5, E_g values of S_1 to S_4 are 3.25, 3.23, 2.16, and 0.92 eV, respectively. E_g decreases as L increases. When L≥5, E_g values increase. To understand the physical background of the above change, the band structures and part density of state (PDOS) of ZnO and CuO SWNTs (for a comparison purpose) are given in Fig. 2b and c, respectively. In the left part of Fig. 2b, the blue (black) curves represent spin up (down). In the PDOS curves of Fig. 2c, the black line shows the total density of states of ZnO or CuO SWNTs. The olive, red and blue curves denote PDOS of Zn/Cu-3d, O-2p, Zn/Cu-4s orbits, respectively.

According to our previous work [22], in ZnO SWNT, Zn-3d Zn-4s and O-2p orbits and in the CuO SWNT, the Zn-4s, Cu-3d, Cu-4s and O-2p orbits play important roles around Fermi level (E_F), respectively. Thus, the effect of above orbits to the band gap variation is considered in our configurations in this work.

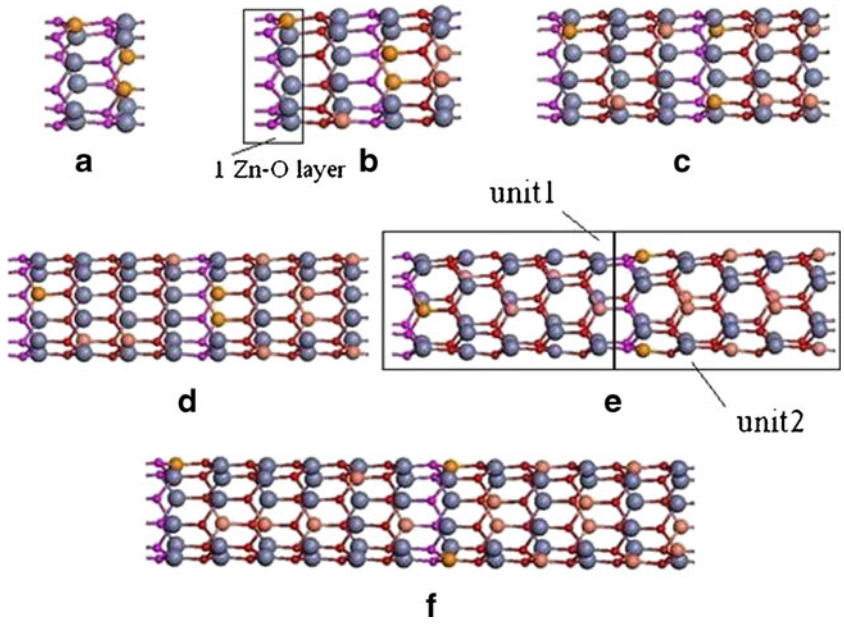

Fig. 1 A ball and stick structure of $(Zn_{4/6}Cu_{2/6}O)_L$/$(Zn_{5/6}Cu_{1/6}O)_L$, where small (red), large (gray), and middle (orange) balls show O, Zn and, Cu atoms, respectively. **a** S_1, **b** S_2, **c** S_3, **d** S_4, **e** S_5, **f** S_6

The band structures and PDOS of S_1 to S_6 are displayed in Fig. 3. For S_1, S_2 and S_6 in Fig. 3a, b and f, the variation tendencies are similar. CBM decreases obviously and VBM increases little compared to the original one. The energy levels above E_F are contributed not only by Cu-3*d* orbit but also partly by O-2*p* orbit. The difference is there are energy band splitting and the broadening of O-2*p* and Zn-4*s* orbits in S_1 not in the others.

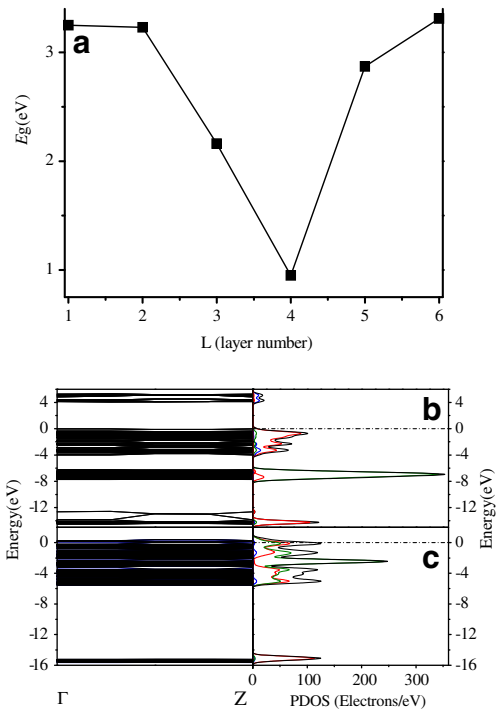

Fig. 2 E_g of $(Zn_{4/6}Cu_{2/6}O)_L$/$(Zn_{5/6}Cu_{1/6}O)_L$ as a function of L (**a**). Band structure and the corresponding DOS and PDOS of Zn-4*s*, Zn-3*d*, O-2*s* and O-2*p* orbits in ZnO SWNT (**b**), and that of Cu-4*s*, Cu-3*d*, and O-2*p* orbits in CuO SWNT (**c**). The black, red, blue and violet curves show the part density of states Cu-3*d*, O-2*p*, Zn-4*s* and Cu-4*s* orbits, respectively

The band structure and corresponding PDOS of S_3 and S_5 are shown in Fig. 3c and e. In these cases of L=3 and 5, the band structure variation is so different from the above three cases. CBM contributed by Zn-4*s* and O-2*p* orbits decreases. Meanwhile, the single DOS peak of CB splits into double ones with energy band broadening. VBM, made by two new energy high levels named as 1st and 2nd levels, increases remarkably when they are compared to the above configurations. The right part of Fig. 3c presents the corresponding PDOS of the two levels of Cu-3*d* and O-2*p* orbits. In light of the figure, VBM is affected by not only the substituted Cu atoms, but also the corresponding variety of O layers. In the band structure and PDOS of S_5, the decrease of CBM is not as obvious as that of S_3. VBM made by five new energy high levels increases.

For S_4 is also appeared an interesting variation shown in Fig. 3d with $E_g(S_4)$=0.95 eV, the drop of conduction band (CB) is largest where the energy band splitting and broadening of O-2*p*, Zn-4*s* and Cu-4*s* orbits in CB is most obvious among all structures. Zn-4*s* orbits split into three peaks in CB, which differs from other configurations. An increase of VBM is similar to that of S_2. The energy levels near E_F are contributed not only by Cu-3*d* orbits, but also by O-2*p* orbits partly. Another character of the band structure of S_4 is the coincidence of spin up and down levels. There will be unpaired lone electrons in the process of Cu substituting Zn site in ZnO SWNT, which separates spin up and down levels. It is obvious that the ability of bounding electrons of Cu is weaker than Zn. Therefore, some electrons in S_4 are in freedom states.

To understand the fact that E_g is different in distinct configurations, the PDOS of Zn, Cu, and O of each layer

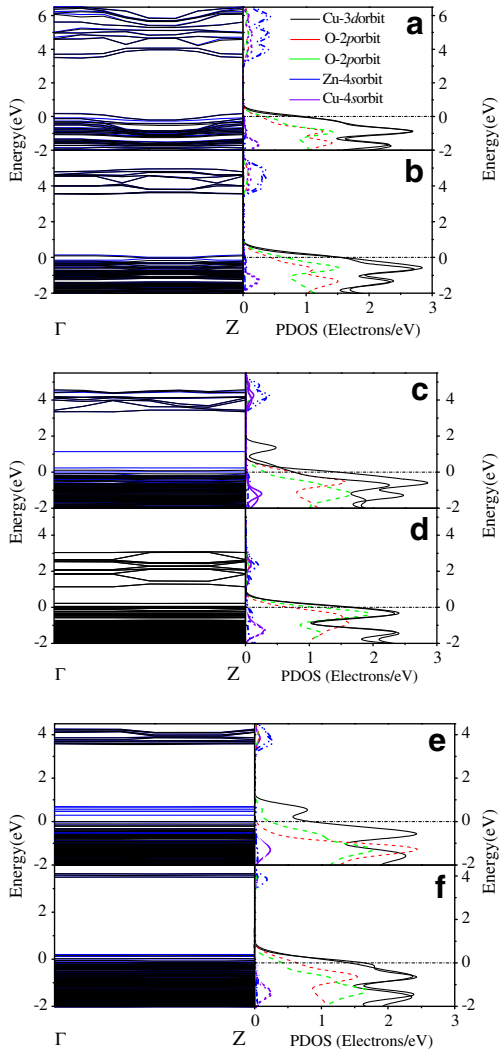

Fig. 3 Band structure and the corresponding DOS and PDOS of Zn-4*s*, Zn-3*d*, O-2*s* and O-2*p* orbits for S_1 (**a**), S_2 (**b**), S_3 (**c**), S_4 (**d**), S_5 (**e**), and S_6 (**f**). The black, red, blue and violet curves show the part density of states Cu-3*d*, O-2*p*, Zn-4*s* and Cu-4*s* orbits, respectively

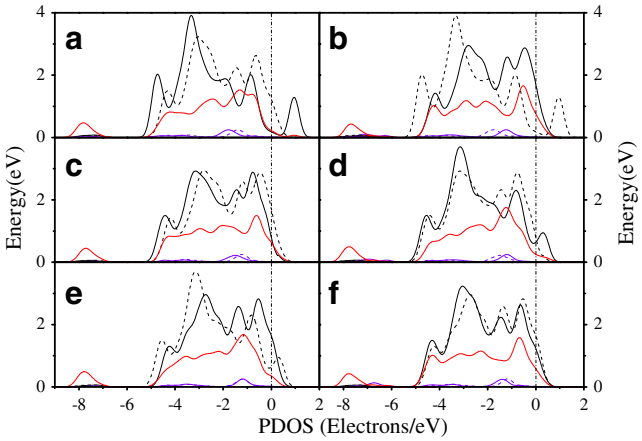

Fig. 4 The PDOS of O-2*p*, Cu-4*s*, and Cu-3*d* orbits of each single layer. **a** the O-2*p* orbits of 1st O layer and Cu-4*s*, Cu-3*d* orbits of 1st and 6th Zn/Cu layer. **b** the O-2*p* orbits of 2nd O layer and Cu-4*s*, Cu-3*d* orbits of 2nd and 1st Zn/Cu layer. (**c**) the O-2*p* orbits of 3rd O layer and Cu-4*s*, Cu-3*d* orbits of 3rd and 2nd Zn/Cu layer. **d** the O-2*p* orbits of 4th O layer and Cu-4*s*, Cu-3*d* orbits of 4th and 3th Zn/Cu layer. **e** the O-2*p* orbits of 5th O layer and Cu-4*s*, Cu-3*d* orbits of 5th and 4th Zn/Cu layer. **f** the O-2*p* orbits of 6th O layer and Cu-4*s*, Cu-3*d* orbits of 6th and 5th Zn/Cu layer. The black, red, blue and violet curves show the part density of states Cu-3*d*, O-2*p*, Zn-4*s* and Cu-4*s* orbits, respectively. The solid lines indicate that of U1 and the dot lines indicate that of U2

in S_3 and S_4 are given in Figs. 4 and 5 as examples. Since each single O layer bonds with left and right two single Zn/Cu layers, PDOS curves are contributed by the O layer and the left and right Cu layers. As mentioned above, VBM of S_3 is contributed by Cu-3*d* and O-2*p* orbits. To identify the bonding between Cu and O, the PDOS of Cu-4*s*, Cu-3*d* and O-2*p* orbits are given in Fig. 4. For S_3, the 1st and 4th O layers bond Zn/Cu layers combined with one and two Cu atoms, respectively. It is definite that the interface between U1 and U2 includes three single layers: Zn/Cu layer with one Cu atom, Zn/Cu layer with two Cu atoms, and the O layer bonding with them. According to this definition, the middle layers are the 2nd Zn/Cu single layer, 5th Zn/Cu single layer and the O single layers bonding with them in S_3.

In Fig. 4a, the red, violet and black solid curves represent O-2*p*, Cu-4*s* and Cu-3*d* orbits of 1st O and 1st Zn/Cu layers, respectively. Figure 4a and d are the bonds at interface layers, Fig. 4b, c, d and e are the bonds between interface and middle layers. The O-2*p* orbits of 1st O layer bond with Cu-4*s* and Cu-3*d* orbits of 1st Zn/Cu layer at -9 to -7 eV, and that of 6th Zn/Cu layer at -2 to -1 eV, but not that at -5 to 0 eV. New antibonding orbits formed above E_F are mainly contributed by unoccupied Cu-3*d* orbits. A similar case appears at 4th Zn-O layer.

Bonding among Cu-3*d*, Cu-4*s* and O-2*p* in the middle layers differs from that in the interface layers. Cu-3*d* orbits of 2nd Zn/Cu layer bond with O-2*p* orbits of 2nd layer at -5 to -4 eV and -1 to 0 eV except the region from -9 to -7 eV. The former is a bonding state and the latter is an antibonding state. The nonbonding state is located between them. Cu-3*d* orbits of 2nd Zn/Cu layer bonds with O-2*p* orbits of 3rd layer at -9 to -7 eV while the antibonding states are located at -1 to 0 eV. The bonding between Cu-3*d* orbits of 5th Zn/Cu layer and O-2*p* orbits of 6th/5th O layer is similar to the above.

PDOS of S_4 is given in Fig. 5. Figure 5a and e show the bonding in interface layers while Fig. 5c and g present the bonding in middle layers. Fig. 5b, d, f and h denote the bonding between interface and middle layers. Differing from those of S_3, CB contributed by Zn-4*s*, O-2*p* and Cu-4*s* orbits decreases. The bonding between Zn-4*s* (Cu-4*s*) and O-2*p* has the characteristic of CuO SWNT from -8 to -6 eV, while that has the characteristic of ZnO SWNT between -4 to 0 eV. However, those of Cu are divided into two

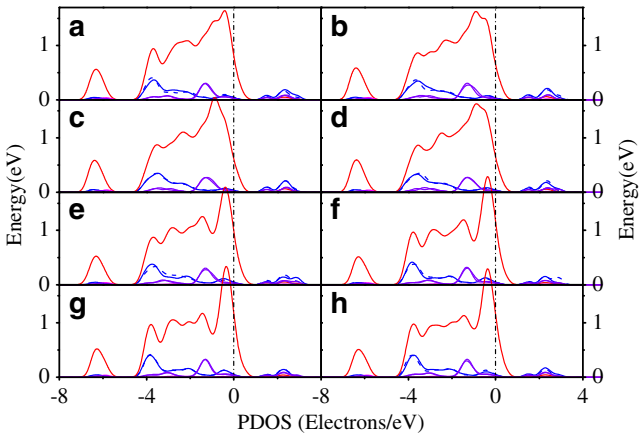

Fig. 5 PDOS of O-2*p*, Cu-4*s*, and Cu-3*d* orbits of each single layer. **a** O-2*p* orbits of 1st O layer and Cu-4*s*, Zn-4*s* orbits of 1st and 8th Zn/Cu layer. **b** O-2*p* orbits of 2nd O layer and Cu-4*s*, Zn-4*s* orbits of 2nd and 1st Zn/Cu layer. **c** O-2*p* orbits of 3rd O layer and Cu-4*s*, Zn-4*s* orbits of 3rd and 2nd Zn/Cu layer. **d** O-2*p* orbits of 4th O layer and Cu-4*s*, Zn-4*s* orbits of 4th and 3th Zn/Cu layer. **e** O-2*p* orbits of 5th O layer and Cu-4*s*, Zn-4*s* orbits of 5th and 4th Zn/Cu layer. **f** O-2*p* orbits of 6th O layer and Cu-4*s*, Zn-4*s* orbits of 6th and 5th Zn/Cu layer. **g** O-2*p* orbits of 7th O layer and Cu-4*s*, Cu-3*d* orbits of 7th and 6th Zn/Cu layer. **h** O-2*p* orbits of 8th O layer and Cu-4*s*, Cu-3*d* orbits of 8th and 7th Zn/Cu layer. The black, red, blue and violet curves show the part density of states Cu-3*d*, O-2*p*, Zn-4*s* and Cu-4*s* orbits, respectively

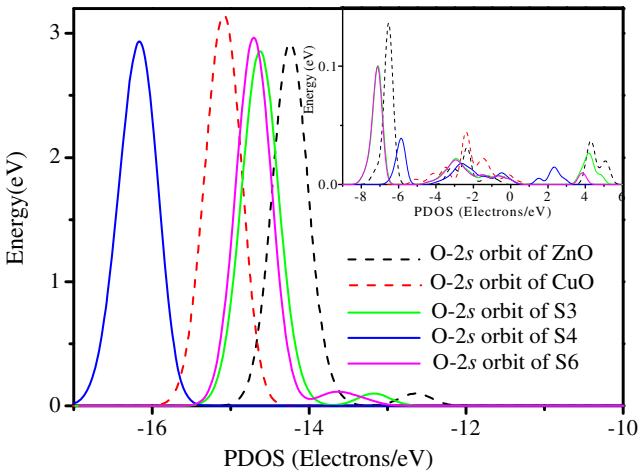

Fig. 6 The PDOS of O-2*s* orbits of S_3, S_4, S_6, ZnO SWNT and CuO SWNT. The black, red, green, blue and pink curves show the part density of states O-2*s* orbits of ZnO SWNT, CuO SWNT, S_3, S_4 and S_6, respectively

parts of U1 and U2 but not interface and middle layers. Cu-4*s* and O-2*p* bonding in U1 is little while that from -2 to 0 eV in U2 is similar to that of CuO SWNT. In summary, E_g of S_4 is similar to that of CuO where CB decreases rapidly.

It is known that *sp* hybridization appears in the process of O bonding with metals. Lone pairs contributed by O-2*s* and O-2*p* orbits play an important role in forming antibonding states [41]. The O-2*p* orbits have been discussed above; here consider O-2*s* orbits, which are related to the decrease of CB in S_4, and differs from others. The PDOS of O-2*s* orbits of S_3, S_4, S_6 for ZnO SWNT and CuO SWNT are shown in Fig. 6. It is shown that O-2*s* orbits of S_4 are separated in comparison with those of S_3 and S_6. They are more localized than the others, being closer to that of CuO but not to that of ZnO. The change of lone pairs may induce the formation of dipole, which drops the antibonding orbits above E_F.

For S_1 and S_2, no or one middle layer is present, which leads to that the case is similar to symmetrical doping. S_5 and S_6 have more than two middle layers, which results in less interface effect. Both cases have similar E_g values.

Thus, the band gap can be modulated by our method alloying through constructing an appropriate variation period. The results show that the band gap appears the minimum in S_4 (L=4) which has been near the conductor. The band gaps of S_3 (L=3) and S_5 (L=5) also decrease obviously compared to the other three configurations. Especially, the band gap of S_3 has decreased to 2.16 eV which is in the region of narrow bandgap semiconductor. Since the band gap of ZnO SWNT is wide, it mainly absorbs light in UV region. It is well known that ultraviolet light accounts for only about 5 % of solar energy. Our ZnCuO superlattices with these band gap values can absorb light in both visible light and UV region. These properties make the superlattices a potential application in photocatalysis and the visible light emitter.

Conclusions

The effect of interface and middle layers on the band gap are considered in the variation of periodic $(Zn_{4/6}Cu_{2/6}O)_L/(Zn_{5/6}Cu_{1/6}O)_L$ superlattices by changing the size of L. The variation tendency of band gap appears a minimum in S_4 (L=4) which has been near the conductor. The band gaps of S_3 (L=3) and S_5 (L=5) also decrease obviously compared to the other three configurations. Especially, the band gap of S_3 has decreased to 2.16 eV which is in the region of narrow bandgap semiconductor. The middle layer can induce the VBM increase or CBM decrease rapidly. The band gap can be modulated by alloying through constructing an appropriate variation period, and these properties make the superlattices a potential application in photocatalysis and the visible light emitter.

Acknowledgments Authors acknowledge the supports by National Key Basic Research and Development Program (Grant No. 2010CB631001) and by Program for Changjiang Scholars and Innovative Research Team in University, and High Performance Computing Center (HPCC) of Jilin University.

References

1. Shah SM, Martini C, Ackermann J, Fages F (2012) Photoswitching in azobenzene self-assembled monolayers capped on zinc oxide: nanodots vs nanorods. J Colloid Interface Sci 367:109–114
2. Panigrahy B, Aslam M, Bahadur D (2012) Effect of Fe doping concentration on optical and magnetic properties of ZnO nanorods. Nanotechnology 23:115601
3. Chen HN, Zhu LQ, Liu HC, Li WP (2012) Growth of ZnO nanowires on fibers for one-dimensional flexible quantum dot-sensitized solar cells. Nanotechnology 23:075402
4. Wang LH, Liu HZ, Qian J, Yang WG, Zhao YS (2012) Structural stability and compressibility study for ZnO nanobelts under high pressure. J Phys Chem C 116:2074–2079
5. Chai GLL, Zhou J, Lin CS, Yang Y, Cheng WD (2012) Second-order optical response of single-walled zinc oxide nanotubes from first principles calculations. Chem Phys Lett 529:49–53
6. Pelatt BD, Huang CC, Conley JF (2010) ZnO nanobridge devices fabricated using carbonized photoresist. J Solid State Electron 54:1143–1149
7. Yi GC, Wang C, Park WI (2005) ZnO nanorods: synthesis, characterization and applications. Semicond Sci Technol 20:S22–S34
8. Arnold MS, Avouris P, Pan ZW, Wang ZL (2003) Field-effect transistors based on single semiconducting oxide nanobelts. J Phys Chem B 107:659–663
9. Huang MH, Mao M, Feick H, Yan HQ, Wu YY, Kind H, Weber E, Russo R, Yang PD (2001) Room-temperature ultraviolet nanowire nanolasers. Science 292:1897–1899
10. Keem K, Kim H, Kim GT, Lee JS, Min B, Cho K, Sung MY, Kim S (2004) Photocurrent in ZnO nanowires grown from Au electrodes. Appl Phys Lett 84:4376–4378
11. Lee CJ, Lee TJ, Lyu SC, Zhang Y, Ruh H, Lee HJ (2002) Field emission from well-aligned zinc oxide nanowires grown at low temperature. Appl Phys Lett 81:3684–3650
12. Ajayan PM, Stephan O, Colliex C, Trauth D (1994) Aligned carbon nanotube arrays formed by cutting a polymer resin-nanotube composite. Science 265:1212–1214
13. Banerjee SS, Wong SS (2002) Synthesis and characterization of carbon nanotube-nanocrystal heterostructures. Nano Lett 2:195–200
14. Shin HJ, Jeong DK, Lee JG, Lee JG, Sung MM, Kim JY (2004) Formation of TiO2 and ZrO2 nanotubes using atomic layer deposition with ultraprecise control of the wall thickness. Adv Mater 16:1197
15. Xie SY, Wang W, Fermando KAS, Wang X, Lin Y, Sun YP (2005) Solubilization of boron nitride nanotubes. Chem Commun 29:3670–3672
16. Samarakoon DK, Wang XQ (2010) Tunable band gap in hydrogenated bilayer graphene. ACS Nano 4:4126–4130
17. Li QH, Gao T, Wang YG, Wang TH (2005) Optoelectronic characteristics of single CdS nanobelts. Appl Phys Lett 86:193109
18. Wan Q, Lin CL, Yu XB, Wang TH (2004) Room-temperature hydrogen storage characteristics of ZnO nanowires. Appl Phys Lett 84:124–126
19. Xing YJ, Xi ZH, Xue ZQ, Zhang XD, Song JH, Wang RM, Xu J, Song Y, Zhang SL, Yu DP (2003) Optical properties of the ZnO nanotubes synthesized via vapor phase growth. Appl Phys Lett 83:1689–1691
20. Hu JQ, Li Q, Meng XM, Lee CS, Lee ST (2003) Thermal reduction route to the fabrication of coaxial Zn/ZnO nanocables and ZnO nanotubes. Chem Mater 15:305–308
21. Zhang X, Zhang Y, Xu J, Wang Z, Chen X, Peculiar YD (2005) Peculiar ZnO nanopushpins and nanotubes synthesized via simple thermal evaporation. Appl Phys Lett 87:123111
22. Song DM, Li JC, Jiang Q (2012) Visible light photocatalysis of single-walled (Zn4/6Cu2/6O)(3)/(Zn5/6Cu1/6O)(3) superlattice nanotube for redox reaction of water calculated by generalized gradient approximations with the Hubbard U model. J Appl Phys 111:034318
23. Tu ZC, Hu X (2006) Elasticity and piezoelectricity of zinc oxide crystals, single layers, and possible single-walled nanotubes. Phys Rev B 74:035434
24. Shen X, Allen BP, Muckerman JT, Davenport JW, Zheng JC (2007) Wire versus tube: stability of small one-dimensional ZnO nanostructures. Nano Lett 7:2267–2271
25. Sun Y, Fuge GM, Fox NA, Riley DJ, Ashfold MNR (2005) Synthesis of aligned arrays of ultrathin ZnO nanotubes on a Si wafer coated with a thin ZnO film. Adv Mater 17:2477
26. Mo XH, Gao J, Goodwin JG (2009) Role of promoters on Rh/SiO2 in CO hydrogenation: a comparison using DRIFTS. Catal Today 147:126–149
27. Schrier J, Demchenko DO, Wang LW (2007) Optical properties of ZnO/ZnS and ZnO/ZnTe heterostructures for photovoltaic applications. Nano Lett 7:2377–2382
28. Lu ZS, Yang ZX (2010) Interfacial properties of NM/CeO2(111) (NM=noble metal atoms or clusters of Pd, Pt and Rh): a first principles study. J Phys Condens Matter 22:475003
29. Vanderbilt D (1990) Soft self-consistent pseudopotentials in a generalized eigenvalue formalism. Phys Rev B 41:7892–7895
30. Delley B (2000) From molecules to solids with the DMol(3) approach. J Chem Phys 113:7756–7764
31. Troullier N, Martins JL (1991) Efficient pseudopotentials for plane-wave calculations. Phys Rev B 43:1993–2006
32. Sun J, Wang HT, He JL, Tian YJ (2005) Ab initio investigations of optical properties of the high-pressure phases of ZnO. Phys Rev B 71:125132
33. Buchholz DB, Chang RPH, Song JH, Ketterson JB (2005) Room-temperature ferromagnetism in Cu-doped ZnO thin films. Appl Phys Lett 87:082504
34. Mao YL, Zhong JX, Chen YP (2008) First principles study of the band structure and dielectric function of (6,6) single-walled zinc oxide nanotube. Physica E 40:499–502
35. Perdew JP, Zunger A (1981) Self-interaction correction to density-functional approximations for many-electron systems. Phys Rev B 23:5048–5079
36. Anisimov VI, Zaanen J, Andersen OK (1991) Band theory and Mott insulators: Hubbard *U* instead of Stoner. Phys Rev B 44:943–954
37. Anisimov VI, Solovyev IV, Korotin MA, Czyzyk M, Sawatzky GA (1993) Density-functional theory and NiO photoemission spectra. Phys Rev B 48:16929–16934
38. Liechtenstein AI, Anisimov VI, Zaanen J (1995) Density-functional theory and strong interactions: Orbital ordering in Mott-Hubbard insulators. Phys Rev B 52:R5467–R5470
39. Lany S, Zunger A (2005) Anion vacancies as a source of persistent photoconductivity in II-VI and chalcopyrite semiconductors. Phys Rev B 72:035215
40. An W, Wu XJ, Zeng XC (2008) Adsorption of O-2, H-2, CO, NH3, and NO2 on ZnO nanotube: a density functional theory study. J Phys Chem C 112:5747–5755
41. Tiago ML, Chan TL (2004) Metal-dimer atomic reconstruction leading to deep donor states of the anion vacancy in II-VI and chalcopyrite semiconductors. Phys Rev Lett 93:156404